

# Enhancing FRET through DNA-controlled Emitters and ENZ Metamaterials

Akeshi Aththanayeke Andrew Lininger Anh Pham Radu Malureanu Divita Mathur\* Giuseppe Strangi\*

A. Aththanayeke, A. Lininger, A. Pham

Department of Physics, Case Western Reserve University, Cleveland OH, USA

R. Malureanu

Department of Electrical and Photonics Engineering, Technical University of Denmark, Copenhagen, Denmark

National Centre for Nano Fabrication and Characterization, Technical University of Denmark, Copenhagen, Denmark

D. Mathur

Department of Chemistry, Case Western Reserve University, Cleveland OH, USA

email: divita.mathur@case.edu

G. Strangi

Department of Physics, Case Western Reserve University, Cleveland OH, USA

Department of Physics, NLHT Lab - University of Calabria and CNR-NANOTEC Istituto di Nanotecnologia, Rende, Italy

email: giuseppe.strangi@case.edu

Keywords: *epsilon-near-zero, ENZ, FRET, DNA origami, light-matter interactions, nanophotonics, energy transfer, metamaterials*

The ability to significantly enhance energy transfer processes at the nanoscale requires the simultaneous optimization of molecular scale orientation and macroscopic photonic enhancement between multiple quantum emitters. However, achieving this dual control has remained a significant experimental challenge, often limited by the stochastic arrangement of emitter assemblies and spatially non-uniform electromagnetic fields in conventional photonic platforms. In this work, we demonstrate a unified architecture that achieves this synergy by combining the structural precision of DNA nanotechnology with the unique field environment generated by epsilon-near-zero (ENZ) materials. Using DNA molecular beacons as programmable emitter scaffolds, we establish fixed donor-acceptor separations and emitter orientations (Atto425/Cy3.5) in two well-defined conformational states: closed hairpin (emitter separation 2 nm), and open extended (7.2 nm) configurations. These structures are then embedded in the near-field of a multilayer ENZ metamaterial substrate, which facilitates spatially uniform, enhanced electromagnetic field coupling. Time-resolved photoluminescence measurements demonstrate a significant increase in FRET efficiency for DNA-programmed emitter pairs in the ENZ environment, compared to those on a glass substrate, corresponding to increased donor quenching and shortened donor lifetime. These results establish a scalable experimental pathway for engineering light-matter interactions at molecular scales, enabled by the structural precision of DNA paired with ENZ mediated redistribution of the local density of optical states (LDOS) to amplify near-field coupling between quantum emitters, with applications in next-generation bio-sensing and quantum photonic technologies.

## 1 Introduction

The ability to manipulate light-matter interactions at the nanoscale is central to the development of next generation photonic and quantum optical technologies [1, 2, 3, 4, 5]. Modern *classical* communication systems can tolerate substantial microscopic disorder since information is encoded and recovered in the averaged, macroscopic response of engineered channels [6]. In contrast, *quantum* communication relies on precisely controlling fundamental energy and information transfer processes between discrete emitters, including resonance energy transfer, coherent dipole-dipole coupling, and collective emission [7, 8, 9]. These processes depend sharply on factors such as emitter separation and relative orientation, and the local electromagnetic environment [10]. This inherent sensitivity makes scalable and reliable quantum links difficult to realize, and represents a fundamental challenge in translating quantum science into functional devices [11, 12]. In conventional dielectric environments, the local electromagnetic field near an emitter can exhibit high spatial variability, which makes the efficiency of energy transfer processes strongly position dependent [13] and can degrade performance. Furthermore, simultaneous control over relative emitter spacing and dipole orientation is typically difficult to achieve at the relevant length scales, often leading to significant disorder. These disordered systems may be described by stochastic distributions of emitter

arXiv:2602.20509v1 [physics.optics] 24 Feb 2026

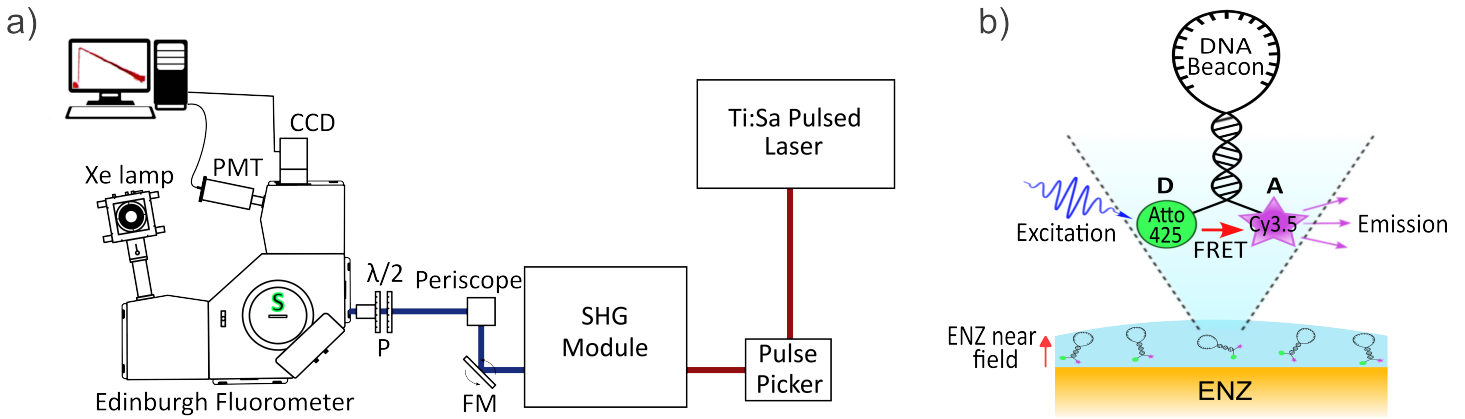


Figure 1: Experimental implementation and system description: a) Experimental layout for steady-state and time-resolved spectroscopy. b) Schematic of DNA beacon-based spatial locking of the donor-acceptor pair. Dye-labeled MBs are embedded in a thin PVA film on the ENZ multilayer, positioning fixed-distance FRET pairs within the ENZ near field.

separation and orientation, however broad emitter distributions inherently undermine and obscure the fundamental physics underlying coupling efficiency, effectively ‘smearing’ the geometric properties of the population, and therefore measured performance, from the optimized physical limits of the photonic environment [14]. Thus, nominally identical devices can exhibit drastically different behaviors or consistently suboptimal performance, and small separation and orientation misalignment can dominate the observed efficiency [15].

ENZ materials are a special class of metamaterials in which the real part of the effective permittivity approaches zero at a designed resonance frequency [16, 17], generating an engineered electromagnetic environment that can amplify and mediate emitter coupling. For electromagnetic waves with frequencies near the ENZ point, the wavelength inside the material becomes effectively infinite, and the phase advance is suppressed, producing highly spatially uniform electromagnetic fields across extended regions [18, 19]. Although many photonic platforms can mediate emitter coupling through discrete resonant mode enhancement, including plasmonic nanostructures, these approaches typically produce strongly localized, spatially nonuniform hotspots [20], which makes precise emitter placement and reproducible coupling difficult. In contrast, ENZ platforms can provide broad-area enhancement of the local density of optical states (LDOS)[21, 22] while operating in a slow light regime that mediates the interaction between emitters with low dephasing. This combination makes ENZ systems particularly attractive for studying dipole-dipole processes such as Förster resonance energy transfer (FRET). Theoretical studies predict that ENZ media can enhance and extend the effective range of resonance energy transfer beyond the conventional  $1/r^6$  scaling [23, 24]. However, even with ENZ photonic enhancement, the degree of energy transfer cannot be optimized without strongly controlling the relative emitter spacing and orientation, as described above [25]. One approach to overcome the limitations of stochastic emitter placement is to employ DNA-programmable architectures that enable nanometer-precision control of emitter spacing and, in selected geometries, their relative orientation. Such bottom-up assembly strategies remove geometric uncertainty and allow systematic interrogation of distance-dependent interactions.

DNA nanotechnology can provide the missing link of molecular scale control to fully optimize energy transfer processes. Over the past several decades, synthetic DNA has transitioned from a genetic carrier to a highly successful structural building block, used to engineer complex architectures with sub nanometer precision [26, 27, 28, 29]. In particular, DNA based ‘molecular rulers’ have been widely successful in biological sensing and structural characterization, where they impose nanometer-scale separations with minimum configurational degrees of freedom [30]. These scaffolds have demonstrated highly reproducible emitter placement control, including for energy transfer processes such as Förster Resonance Energy Transfer (FRET), across various dye networks, greatly decreasing the stochasticity present in other approaches [31]. Beyond purely organic fluorophores, DNA-templated assembly has enabled the development of sophisticated hybrid nanophotonic systems, leveraging precise spatial control to engineer plasmonic resonances and enhance light-matter interactions at the nanoscale [32, 33]. One such structure is the DNA molecular

beacon (MB), which consists of a single stranded oligonucleotide sequence that naturally hybridizes to form a stable hairpin structure with a ‘loop’ flanked by two complementary ‘stem’ sequences [31]. In this state (closed), fluorophores attached to the ends are brought into close proximity. However, upon hybridization with a target/complimentary strand, the hairpin structure opens into an extended, rigid double helix configuration (opened), significantly increasing the donor-acceptor separation [34]. This introduces a bistable ‘locking’ mechanism with fixed emitter separation and relative orientation [35, 36].

In this study, the deterministic DNA-defined emitter placement and ENZ optical field engineering approaches are unified to enhance molecular energy transfer within the visible spectrum beyond the typical limit of singular photonic or geometric enhancement. The DNA MB structure described above is employed to fix the donor-acceptor (Atto425/Cy3.5) separations in two structurally enforced conformational states: a closed hairpin (emitter separation 2 nm) and an opened (extended) configuration (7.2 nm), reducing the geometric uncertainty and stochastic ‘noise’ inherent in traditional flexible linker systems. These DNA structures are then incorporated into the near-field of a multilayer Au/TiO<sub>2</sub> ENZ platform, tuned to coincide with the emitter overlap spectral region. Steady-state fluorescence and time-resolved photoluminescence (TRPL) measurements are performed to quantify the effects of both DNA-placement and ENZ enhancement of the local density of optical states (LDOS). Ultimately, this work establishes a pathway for the development of reproducible, scalable quantum photonic architectures and next-generation biosensing platforms that largely mitigate nanoscale assembly disorder.

## 2 Experimental Methods

### 2.1 Experimental Implementation

The influence of the ENZ substrate on energy transfer was evaluated using a unified spectroscopic platform that synchronized steady-state fluorescence spectroscopy and time-resolved photoluminescence decay measurements. As illustrated in the measurement workflow in **Figure 1a**, spectral quenching signatures, steady-state fluorescence emission were recorded using a customized Edinburgh fluorometer. The excitation was provided by a Xenon (Xe) lamp set to the donor absorbance range (320-420 nm), a region where direct excitation of the Cy3.5 acceptor is negligible. These spectra were collected over the visible range via a CCD detector to quantify donor quenching across both molecular beacon (MB) conformations.

To resolve sub-nanosecond decay dynamics of the dipole-dipole coupling, the system utilized a time-correlated single-photon counting (TCSP) configuration. The excitation path originated from a pulsed Ti:Sapphire laser (average power of 3W with, 80 MHz repetition rate), regulated by a pulsed picker before entering a Second-Harmonic Generation (SHG) module to achieve the required excitation wavelengths. The beam was then steered through a periscope and a half-wave plate ( $\lambda/2$ ) to control the excitation state before reaching the sample (S) through the polarizer (P). Emission is collected in a perpendicular geometry through a 455 nm long pass filter, which isolates the donor emission channel by suppressing the scattered excitation light. A photomultiplier tube (PMT) recorded the resulting decay curves with measured instrument response function (IRF) of 46 ps. By correlating these dynamic decay behaviors with steady-state data, FRET efficiency was determined directly, ensuring observed enhancements were attributed to the ENZ modified local density of optical states rather than geometric variations.

### 2.2 System Description

The experimental system consists of DNA-programmed molecular beacons (MBs) positioned in the near field of an ENZ substrate, as shown in the general illustration in **Figure 1b**. These MBs provide two well-defined molecular conformations: a closed hairpin state with a donor-acceptor separation of approximately 2 nm, and an opened extended state with a separation of approximately 7.2 nm. This controlled distance pair is specifically chosen to probe ENZ mediated interaction range, since conventional  $1/r^6$  FRET scaling predicts strong quenching at the larger separation, allowing direct assessment of any ENZ enabled extension of dipole coupling. To ensure structural stability and uniform dispersion, the MBs were embedded in 90 nm polyvinyl alcohol (PVA) matrix mixed with 25 mM NaCl. This mixture is deposited using a two-step

spin-coating process (5000 rpm for 5 s, followed by 500 rpm for 5 s [37]) onto the substrates and cured at 60°C.

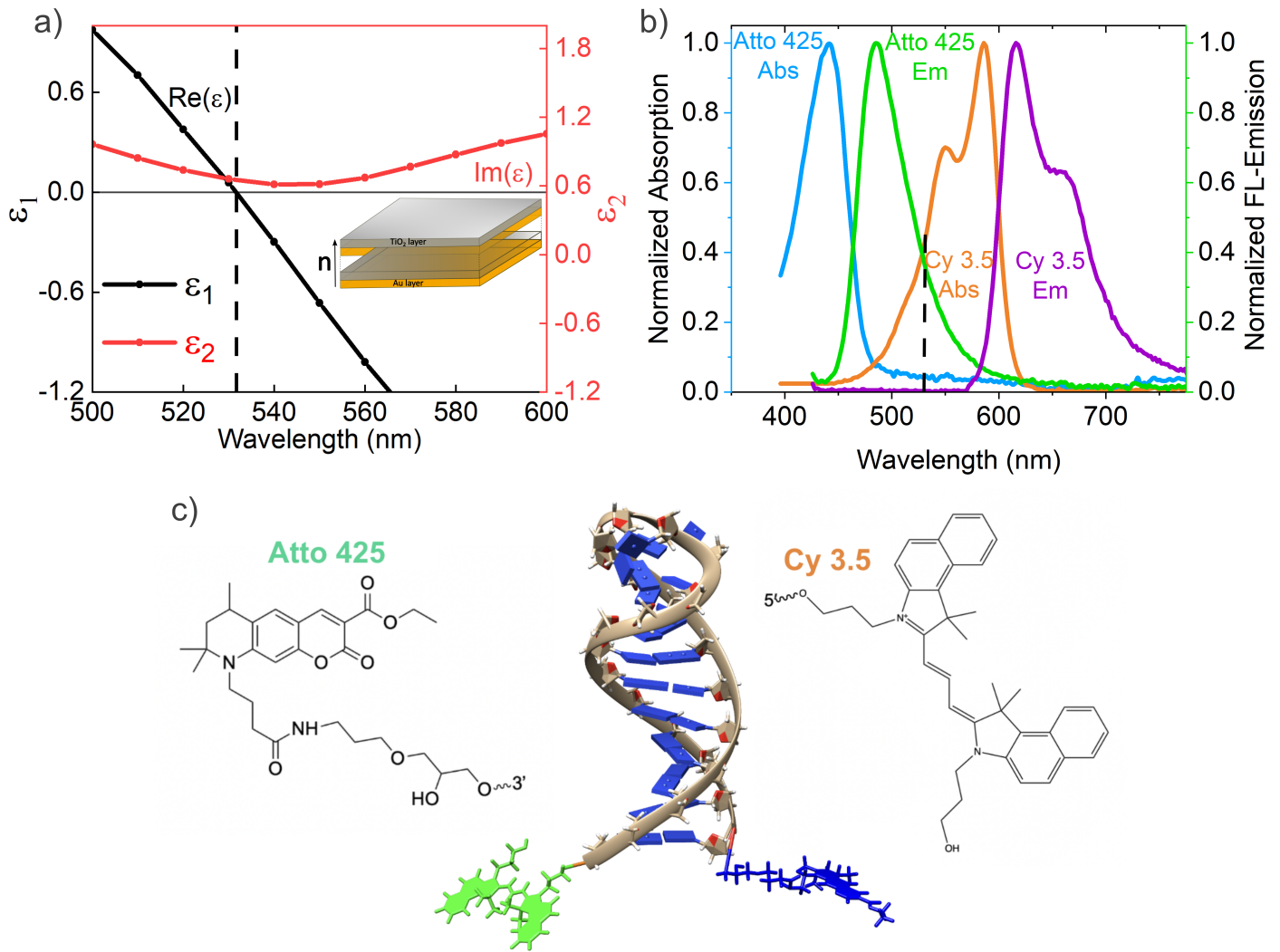


Figure 2: ENZ and fluorophore selection: (a) Schematic cross-section of the Au/TiO<sub>2</sub> multilayer ENZ platform with the ellipsometry data for real and imaginary parts of the permittivity ( $n$ =periodicity for the layers). (b) Normalized donor emission and acceptor absorption spectra showing the donor-acceptor spectral overlap region. (c) Molecular structures of the donor (left) and acceptor (right), with the atomic model of the complete molecular beacon shown in the middle [38] (closed MB configuration).

As illustrated in **Figure 2a**, the ENZ platform is a metal dielectric multilayer specifically engineered so that its ENZ crossing spectrally aligns with the FRET band of the programmed emitters. The structure consists of four ( $n=4$ ) periods of alternating 10 nm Au and 12 nm TiO<sub>2</sub> layers. All the Au and TiO<sub>2</sub> layers were deposited using magnetron sputtering. In the case of TiO<sub>2</sub>, the sputtering was done with added oxygen to ensure the layer's stoichiometry. After each layer deposition, the samples were treated to ensure good adhesion between the Au and the TiO<sub>2</sub> layers [39]. This stack is designed so the effective in-plane permittivity crosses zero at 532 nm, spectrally matching the donor emission and acceptor absorption. AFM characterization of the fabricated multilayer structures reveals very low surface roughness ( $R_a \sim 0.7$ - $0.9$  nm) confirming smooth and conformal PEALD growth. Such low roughness minimizes surface induced scattering and ensures that the optical response is dominated by the designed multilayer geometry rather than by morphological disorder [40]. Spectroscopic ellipsometry verified that the imaginary component of the permittivity remains low at the ENZ point, indicating reduced dissipative loss and enabling stronger field enhancement near the interface.

The suitability of the Atto425/Cy3.5 pair was confirmed through spectral analysis shown in **Figure 2b**. Absorbance measurements showed the donor peak at 439 nm and the acceptor at 550 nm, while emission peaks occur at 488 nm and 610 nm, respectively. This pair provides the substantial spectral overlap necessary for efficient coupling. The structural ‘locking’ of the fluorophores is achieved through the DNA architecture shown in **Figure 2c**. The Atto425 donor is conjugated at the 3’ end via NHS ester chemistry on an amine modification and the Cy3.5 acceptor at the 5’ end via phosphoramidite chemistry on a 24-nucleotide long single stranded DNA oligo. The opened MB was prepared by hybridizing this oligo with a five-fold molar excess of its complementary strand. This ‘locking’ mechanism significantly reduces geometric ambiguity, allowing changes in quenching or lifetime to be attributed directly to the electromagnetic environment. **Table 1** summarizes all the oligos used in this study.

Table 1: List of oligos and the chemical modifications.

Name	Sequence (5’ → 3’)	Modification
MB	GAA TTC GGT ATT TCC TCC GAA TTC	5’Cy3.5; 3’ATTO425
Complementary MB	GAA TTC GGA GGA AAT ACC GAA TTC	N/A
Donor-MB	GAA TTC GGT ATT TCC TCC GAA TTC	3’ATTO425

The combination of structurally well-defined molecular spacing provided by the MB and a spectrally aligned ENZ substrate created a controlled platform for probing how electromagnetic mode redistribution modifies FRET. By positioning the ENZ resonance within the donor emission/acceptor absorption window, the local density of optical states was selectively enhanced, enabling a quantitative investigation of ENZ-mediated modifications to near-field energy-transfer dynamics.

## 3 Results and Discussion

### 3.1 Closed MB

In the closed MB system, efficient energy transfer is expected due to the small donor-acceptor separation. Two sample sets were prepared: a control DNA MB functionalized with only the donor fluorophore (Donor-MB), and the target DNA MB functionalized with both the donor and acceptor fluorophores on the 3’ and 5’ ends, respectively (see **Table 1** for more details). Samples were embedded in thin polymer films ( $\sim 10$  nm) on both glass and ENZ substrates to enable direct comparison of emission behavior in different photonic environments. As shown in **Figure 3a**, photoluminescence (PL) decay curves for the donor-acceptor pair demonstrate a significantly faster decay rate on the ENZ substrate compared to glass (reference). The FRET efficiency was calculated as  $E = 1 - \tau_{DA}/\tau_D$ , where  $\tau_D$  and  $\tau_{DA}$  are the donor lifetimes in the absence and presence of the acceptor, respectively, for the time-resolved analysis [41]. As expected from the short 2 nm separation in the closed MB configuration the energy transfer efficiency is intrinsically high in both environments. The fluorescence decay curve for this emitter pair can be deconvoluted into three distinct  $\tau$  components at different scales, including a fast, sub-nanosecond decay channel. The bar plot in **Figure 3b** highlights the significantly decreased relaxation time (increased decay rate) on the ENZ substrate in each decay channel, relative to the glass substrate. This enhancement is a direct measurement of the modified LDOS near the ENZ surface, which strengthens near-field coupling even at small separation distances. These findings were further corroborated by steady-state fluorescence measurements of the donor-only and donor-acceptor closed MBs when excited at the same wavelength (400 nm). The fluorescence intensity with excitation at the donor emission peak (low acceptor spectral coverage) is shown in **Figure 3c**. In this result, the donor emission intensity, centered at  $\sim 500$  nm is significantly quenched in the presence of the acceptor. The energy transfer efficiency calculated *via* spectral quenching:  $E = 1 - I_{DA}/I_D$ , where  $I_D$  and  $I_{DA}$  are donor fluorescence emission intensities (at the donor emission peak wavelength) in the absence and presence of the acceptor, respectively [41]. This result indicates a  $\sim 90\%$  energy transfer efficiency for the MBs in the solution phase. Such high efficiency confirms the reliability of the closed configuration, as it aligns with the expected dipole-dipole coupling at minimal donor-acceptor separations.

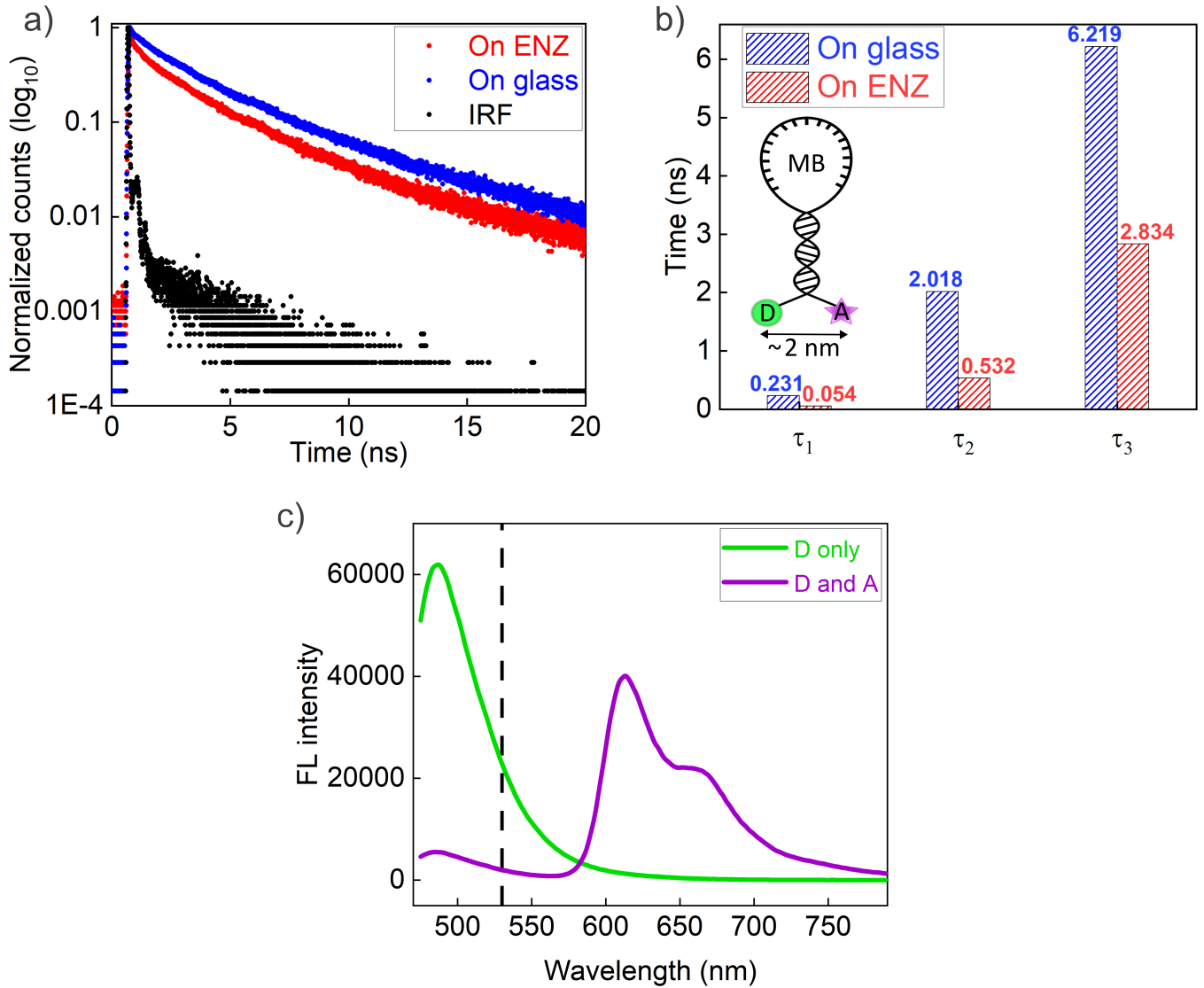


Figure 3: Closed MB system (a) Donor+Acceptor PL decay curves on glass and ENZ substrates (400 nm excitation and 532 emission) (b) Histogram showing the fastened decay on ENZ (c) Steady-state fluorescence emission intensity for the closed donor-MB and for the closed MB systems.

### 3.2 Opened MB

To probe the effect of ENZ photonic enhancement in mediating FRET interactions at increased separation, the opened MB configuration was tested (formed by hybridizing the MB with its complementary oligo, see **Table 1**). In this design, the estimated donor-acceptor separation is approximately 7.2 nm, corresponding to the contour length of the 24-base duplex [42]. Despite the reduced intrinsic coupling at this distance, a pronounced substrate dependence was observed in both the donor only (**Figure 4a**) and donor-acceptor (**Figure 4b**) PL decay curves. The instrument response function (IRF) was measured to be 46 ps and is included in the decay curves for reference. For the donor-only opened MB, the PL decays in glass *versus* ENZ substrate were well described by two components, consistent with the donor's intrinsic relaxation channels with both components being shorter on ENZ. For the donor-acceptor samples, the decays could be explained by three components. The appearance of an additional component suggests the presence of an additional relaxation pathway associated with donor-acceptor interaction under modified photonic conditions; however, further analysis is required to fully assign its physical origin.

The opened MB system exhibited a FRET efficiency of 56.7% on glass and 79.4% on the ENZ substrate. The observed efficiency on the glass substrate is substantially larger than the theoretical  $\sim 21\%$

value predicted for the emitter pair in solution without photonic enhancement or DNA dipole alignment (21%). This discrepancy can be understood quantitatively within the Förster framework. The fundamental equation for efficiency as a function of radius  $r$  is:

$$E = (1 + (r/R_0)^6)^{-1}, \quad (1)$$

where the Förster radius  $R_0$  is given by:

$$R_0^6 \propto \kappa^2 Q_D J n^{-4}, \quad (2)$$

for the orientation factor  $\kappa^2$ , the donor quantum yield  $Q_D$ , and the spectral overlap  $J$  or the local refractive index  $n$  [43]. The quoted value for the theoretical stochastic efficiency (21%) corresponds to a Förster radius  $R_{0,theory} \sim 5.77$  nm, calculated from standard solution parameters with  $r = 7.2$  nm [24]. The observed difference in the experimentally observed efficiency can be interpreted as changes in the effective Förster radius, which can be influenced by each of these factors. Of particular importance for DNA-mediated emitter structures, the emitter pairs in solution assume a random orientation with  $\kappa^2 = 2/3$ . However, this is below the physical maximum of 4 and generally not true in DNA structures where the dipole orientation is fixed. In practice, several thin-film related effects may contribute simultaneously, including: i) restricted rotational freedom and partial dipole alignment due to both the DNA and PVA film (increasing  $\kappa^2$ ); ii) changes in donor quantum yield  $Q_D$  due to suppressed non-radiative channels in the solid matrix; iii) local differences in refractive index compared to aqueous solution; and iv) interface-induced ordering near the glass substrate. These effects could conceivably increase  $R_0$  and hence the observed FRET efficiency at longer distances. In summary, a consistent explanation for the increased efficiency on glass is orientational and photophysical modifications introduced by the thin-film environment [44, 45, 46]. Steady-state fluorescence measurements shown in **figure 4c** also confirmed this value to be 21% efficiency, grounding the reliability of the method.

The essence of this study’s contribution to nanoscale energy transport is summarized in **Figure 4d**. We identify two distinct regimes of enhancement that allow the system to surpass conventional energy transfer boundaries. First, the transition from the stochastic limit, characterized by the broad uncontrolled donor-acceptor distributions found in traditional colloidal systems, to the DNA-mediated enhancement on glass demonstrates the power of the molecular locking mechanism. By constraining the emitters to a fixed 7.2 nm separation within the rigid DNA framework, we establish a reproducible FRET efficiency (57%) that already represents a significant optimization over stochastic assembly.

However, the most critical observation is that this structurally optimized enhancement serves as a baseline or springboard for further photonic enhancement. Upon placing ‘locked’ emitters on the ENZ platform, the FRET efficiency rises (79%), effectively exceeding the non-enhanced limit of the glass control. This secondary leap is driven purely by the macroscopic boundary conditions of the ENZ environment, which reshape the local density of optical states (LDOS) to strengthen dipole-dipole coupling. Critically, this demonstrates that while DNA provides the necessary geometric precision to define the system, the ENZ substrate provides the physical mechanism required to break through conventional efficiency barriers. This unified approach indicates that reaching the highest possible efficiency states requires both molecular scale structural control and engineering electromagnetic environments.

## 4 Conclusion

This study experimentally demonstrates that ENZ environments can significantly enhance dipole-dipole coupling between fluorophores at molecular scales. Using DNA molecular beacons as nanoscale spacers for fixed donor acceptor separations, we observed accelerated donor decay and increased FRET efficiency for both closed (2 nm) and open (7 nm) configurations when the system was placed on a multilayer ENZ substrate. These results provide direct evidence that spatially uniform, boundary condition driven electromagnetic fields of ENZ materials can amplify near field energy transfer beyond conventional distance limited regimes without altering molecular geometry. Additionally, by combining structural precision from

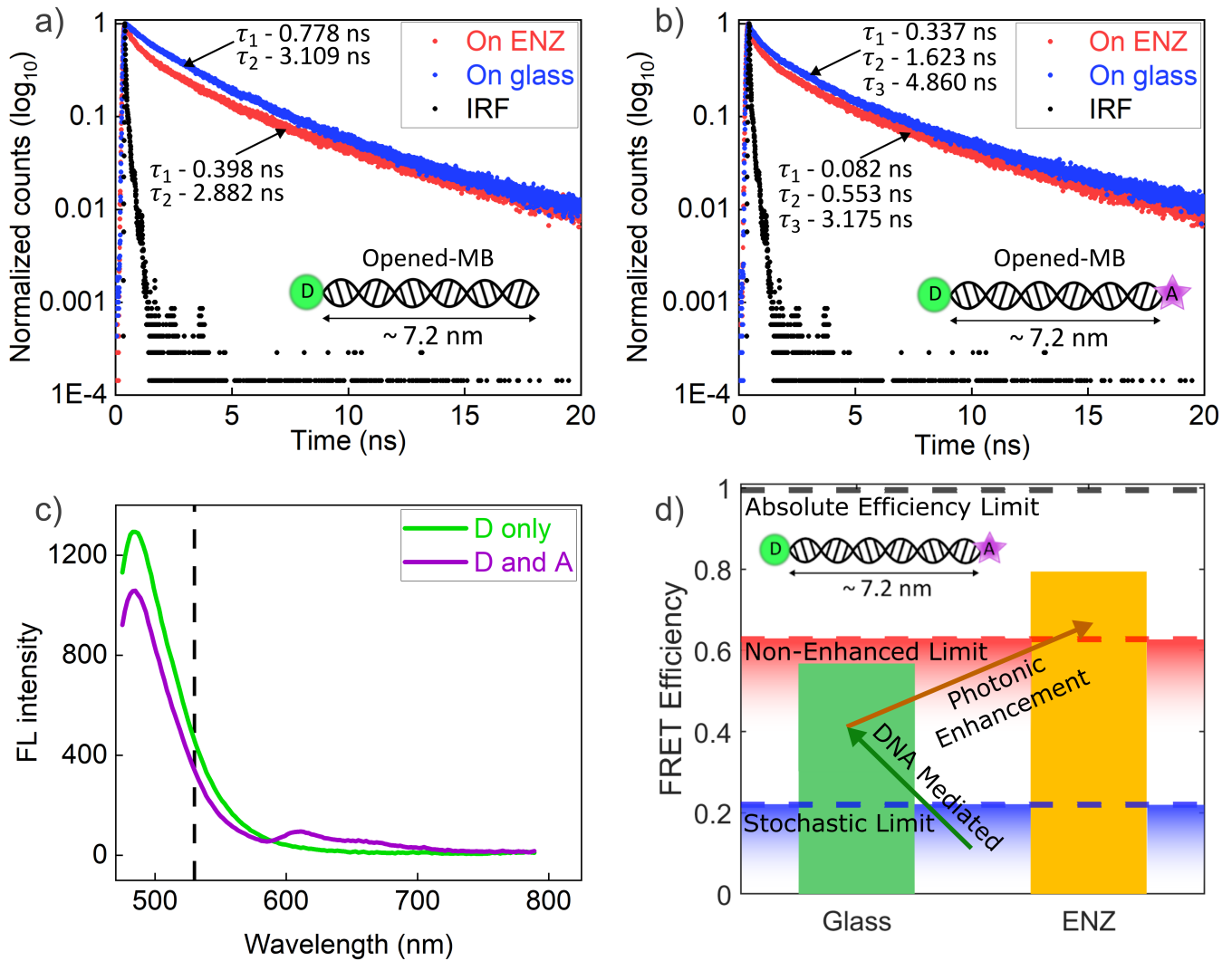


Figure 4: Opened MB system (a) Time-resolved photoluminescence (PL) decay curves for the unfolded beacon containing only the donor dye, measured on a 90 nm polymer film on glass and on the ENZ substrate. (b) PL decay curves for the unfolded beacon containing both donor and acceptor dyes under the same film and substrate conditions (c) Steady-state FL emission opened MB configurations (d) Hierarchical enhancement of energy transfer efficiency, the transition from the stochastic limit (blue dashed line) to the non-enhanced limit on glass (green bar) demonstrates the structural precision provided by DNA locked precision, which overcomes the geometric uncertainty typical of random fluorophore dispersions. The subsequent transition from glass to the ENZ substrate (yellow bar) represents the Photonic enhancement phase.

DNA nanotechnology with engineered photonic environments, this study establishes a robust experimental platform for probing quantum electrodynamic effects in complex optical media. The demonstrated enhancement of FRET without geometrical confinement highlights the potential of ENZ materials for applications in nanoscale light harvesting, biosensing and quantum photonics and provides a pathway toward using macroscopic photonic boundary conditions to actively sculpt molecular-scale energy transport.

### Acknowledgements

The authors acknowledge the use of the Materials for Optoelectronics Research and Education (MORE) Center, a core facility at Case Western Reserve University (est. 2011 via Ohio Third Frontier grant TECH 09-021). The authors acknowledge support from the Ohio Third Frontier Project “Research Cluster on Surfaces in Advanced Materials” (RC-SAM) at Case Western Reserve University. Additionally, authors acknowledge the financial support from the Graduate Student Scholarship and Creative Endeavors (GSSCE) grant provided by the Graduate Council of Arts and Sciences (GCAS) at Case Western Reserve University.

## References

- [1] L. Novotny, B. Hecht, *Principles of nano-optics*, Cambridge university press, **2012**.
- [2] P. Lodahl, S. Mahmoodian, S. Stobbe, *Reviews of Modern Physics* **2015**, *87*, 2 347.
- [3] M. G. Donato, M. Hinczewski, T. Letsou, M. ElKabbash, R. Saija, P. G. Gucciardi, N. Engheta, G. Strangi, O. M. Marago, *arXiv preprint arXiv:2601.10425* **2026**.
- [4] A. Aththanayake, A. Lininger, C. Strangi, M. A. Griswold, G. Strangi, *Nanophotonics* **2025**, *14*, 23 3813.
- [5] A. Lininger, G. Palermo, A. Guglielmelli, G. Nicoletta, M. Goel, M. Hinczewski, G. Strangi, *Advanced Materials* **2023**, *35*, 34 2107325.
- [6] C. E. Shannon, *The Bell system technical journal* **1948**, *27*, 3 379.
- [7] H. J. Kimble, *Nature* **2008**, *453*, 7198 1023.
- [8] R. El-Ganainy, S. John, *New Journal of Physics* **2013**, *15*, 8 083033.
- [9] S. Chattaraj, G. Galli, *Physical Review Research* **2025**, *7*, 3 033229.
- [10] E. M. Purcell, In *Confined electrons and photons: new physics and applications*, 839–839. Springer, **1995**.
- [11] M. O. Scully, M. S. Zubairy, *Quantum optics*, Cambridge university press, **1997**.
- [12] Y. Li, A. Nemilentsau, C. Argyropoulos, *Nanoscale* **2019**, *11*, 31 14635.
- [13] A. F. Koenderink, *ACS photonics* **2017**, *4*, 4 710.
- [14] T. B. Hoang, G. M. Akselrod, M. H. Mikkelsen, *Nano letters* **2016**, *16*, 1 270.
- [15] A. G. Curto, G. Volpe, T. H. Taminiau, M. P. Kreuzer, R. Quidant, N. F. Van Hulst, *science* **2010**, *329*, 5994 930.
- [16] Y. Kiasat, M. G. Donato, M. Hinczewski, M. ElKabbash, T. Letsou, R. Saija, O. M. Maragò, G. Strangi, N. Engheta, *Communications Physics* **2023**, *6*, 1 69.
- [17] K. V. Sreekanth, K. H. Krishna, A. De Luca, G. Strangi, *Scientific reports* **2014**, *4*, 1 6340.
- [18] I. Liberal, N. Engheta, *Nature Photonics* **2017**, *11*, 3 149.
- [19] O. Reshef, I. De Leon, M. Z. Alam, R. W. Boyd, *Nature Reviews Materials* **2019**, *4*, 8 535.
- [20] S. Lal, S. Link, N. J. Halas, *Nature photonics* **2007**, *1*, 11 641.
- [21] P. Xie, W. Wang, Y. Kivshar, *Applied Physics Reviews* **2025**, *12*, 2.
- [22] S. Stengel, J. I. Choi, A. Solanki, H. Ather, P. Chen, B. Triplett, M. Ozlu, K. Choi, A. Senichev, W. Jaffray, et al., *APL Quantum* **2026**, *3*, 1.
- [23] R. Deshmukh, S.-A. Biehs, E. Khwaja, T. Galfsky, G. S. Agarwal, V. M. Menon, *ACS Photonics* **2018**, *5*, 7 2737.
- [24] P. Wu, L. Brand, *Analytical biochemistry* **1994**, *218*, 1 1.
- [25] A. F. Koenderink, A. Alù, A. Polman, *Science* **2015**, *348*, 6234 516.
- [26] D. Mathur, Y. C. Kim, S. A. Diaz, P. D. Cunningham, B. S. Rolczynski, M. G. Ancona, I. L. Medintz, J. S. Melinger, *The Journal of Physical Chemistry C* **2020**, *125*, 2 1509.

- 
- [27] A. K. Adamczyk, T. A. Huijben, M. Sison, A. Di Luca, G. Chiarelli, S. Vanni, S. Brasselet, K. I. Mortensen, F. D. Stefani, M. Pilo-Pais, et al., *ACS nano* **2022**, *16*, 10 16924.
- [28] M. N. Scott, J. L. Banal, W. Jia Chen, C. Brooks, X. Wang, S. M. Hart, A. Dodin, M. Bathe, A. P. Willard, G. S. Schlau-Cohen, *ACS nano* **2025**, *19*, 44 38509.
- [29] D. Mathur, S. A. Díaz, N. Hildebrandt, R. D. Pensack, B. Yurke, A. Biaggne, L. Li, J. S. Melinger, M. G. Ancona, W. B. Knowlton, et al., *Chemical Society Reviews* **2023**, *52*, 22 7848.
- [30] P. W. Rothmund, *Nature* **2006**, *440*, 7082 297.
- [31] S. Tyagi, F. R. Kramer, *Nature biotechnology* **1996**, *14*, 3 303.
- [32] A. O. Govorov, Z. Fan, P. Hernandez, J. M. Slocik, R. R. Naik, *Nano letters* **2010**, *10*, 4 1374.
- [33] A. Kuzyk, R. Schreiber, Z. Fan, G. Pardatscher, E.-M. Roller, A. Högele, F. C. Simmel, A. O. Govorov, T. Liedl, *Nature* **2012**, *483*, 7389 311.
- [34] G. Bonnet, S. Tyagi, A. Libchaber, F. R. Kramer, *Proceedings of the National Academy of Sciences* **1999**, *96*, 11 6171.
- [35] D. Mathur, A. Samanta, M. G. Ancona, S. A. Díaz, Y. Kim, J. S. Melinger, E. R. Goldman, J. P. Sadowski, L. L. Ong, P. Yin, et al., *ACS nano* **2021**, *15*, 10 16452.
- [36] C. Steinhauer, R. Jungmann, T. L. Sobey, F. C. Simmel, P. Tinnefeld, *Angewandte Chemie International Edition* **2009**, *48*, 47 8870.
- [37] M. Kozlov, *Ultra-thin films of polyvinyl alcohol on hydrophobic surfaces: preparation, properties, chemistry, and applications*, University of Massachusetts Amherst, **2004**.
- [38] J. Abramson, J. Adler, J. Dunger, R. Evans, T. Green, A. Pritzel, O. Ronneberger, L. Willmore, A. J. Ballard, J. Bambrick, et al., *Nature* **2024**, *630*, 8016 493.
- [39] J. Sukham, O. Takayama, A. Lavrinenko, R. Malureanu, *ACS applied materials & interfaces* **2017**, *9*, 29 25049.
- [40] R. Malureanu, A. Lavrinenko, *Nanotechnology Reviews* **2015**, *4*, 3 259.
- [41] I. L. Medintz, N. Hildebrandt, *FRET-Förster resonance energy transfer: from theory to applications*, John Wiley & Sons, **2013**.
- [42] J. D. Watson, F. H. Crick, *Nature* **1953**, *171*, 4356 737.
- [43] J. R. Lakowicz, *Principles of fluorescence spectroscopy*, Springer, **2006**.
- [44] S.-A. Biehs, V. M. Menon, G. Agarwal, *Physical Review B* **2016**, *93*, 24 245439.
- [45] H. Schneckenburger, *Methods and applications in fluorescence* **2020**, *8*, 1 013001.
- [46] G. A. Jones, D. S. Bradshaw, *Frontiers in Physics* **2019**, *7* 100.